GR-AS-97-03

High Frequency Buried Target Imaging

Group Report under Contract N00039-91-C-0082
TD No. 01A3095, High Frequency Buried Target Imaging

Nicholas P. Chotiros

Applied Research Laboratories
The University of Texas at Austin
P.O. Box 8029 Austin, Texas 78713-8029

ADVANCED SONAR GROUP

6 October 1997

Approved for public release;
distribution is unlimited.

Prepared for:
Naval Research Laboratory
Stennis Space Center, MS 39529-5004
under the Environmental Physics for MCM Program

Monitored by:
Space and Naval Warfare Systems Command
Department of the Navy
Arlington, VA 22245-5200

TABLE OF CONTENTS

		Page
LIST OF FIGURES		ii
ABSTRACT		1
1.	INTRODUCTION	1
2.	GHOSTING	3
3.	WARPING	5
4.	FOGGING	13
5.	EXPERIMENT	14
6.	CONCLUSIONS	19
ACKNOWLEDGMENTS		20
REFERENCES		21

LIST OF FIGURES

Figure		Page
1	Acoustic pressure and shear stress levels as a function of depth, at 20 kHz in sand, in response to a 0 dB incident acoustic plane wave at grazing angles (a) 40°, (b) 30°, and (c) 20°	4
2	Illustration of ray paths of fast and slow waves to scattering points of a buried target.	6
3	Illustration of warping in the down-range direction by deflection of raypaths due to ripples in the water-sediment interface.	7
4	Illustration of warping in the cross-range direction by deflection of raypaths due to ripples in the water-sediment interface.	8
5	Estimated image warping statistics of 3 m deep target in a muddy sediment as a function of grazing angle.	10
6	Estimated image warping statistics of 30 cm deep target in a sandy sediment as a function of grazing angle, for (a) fast and (b) slow wave images	11
7	Illustration of image warping of a target 3 m deep in a muddy sediment.	12
8	Image degradation due to fogging in a sandy sediment at depths (a) 3 cm and (b) 15 cm.	15
9	Photograph of experimental acoustic arrays.	16
10	Photograph of target array.	16
11	Experiment: (a) vertical section and (b) plan view	17
12	Configuration of targets and projected vertical sonar beam pattern.	18
13	Acoustic imaging results	18

ABSTRACT

Acoustical imaging can potentially provide a buried object classification capability. The image quality is expected to be a function of sediment type, burial depth, and grazing angle. Image degradation is caused by propagation and scattering processes that can be modeled and experimentally measured. Three physical mechanisms were investigated: ghosting, warping, and fogging. Fogging, caused by backscattering from the sediment, is expected to be the limiting factor. A laboratory experiment was conducted to test the findings but the results were inconclusive.

1. INTRODUCTION

In the vast majority of cases, mines are not deeply buried and, therefore, detectable acoustically. In sands, mines are often buried by scouring to a point where the sand just covers the mine. In soft sediments, mines are buried by impact to a depth determined by the shear strength and density of the sediment. In both cases, the mine is detectable acoustically by sonars operating within the usual band of minehunting frequencies, although at a reduced range. Experimental observations over the past several decades indicate that acoustic energy penetrates into the ocean sediment. Results from previous attempts to approximate the ocean sediment as a liquid or as a viscoelastic solid have been misleading in the prediction of acoustic sediment penetration, particularly at shallow grazing angles. Sediment acoustic interactions are best understood in the light of Biot's theory[1] of acoustic propagation in an elastic porous medium, in which the sediment is treated as a water-saturated porous solid. Theory and experimental evidence indicate that detection is not an insurmountable problem.

Classification is more difficult. A mine tethered in the water or laying on the seabed may be classified visually or acoustically. Visual classification is often

preferred because of the higher quality images. For a buried mine, visual classification is impossible because the sediment is opaque. Acoustic classification through a high resolution sonar remains the most viable avenue. Since sound penetrates the sediment, acoustic classification of a buried mine is possible in principle.

There are two main approaches to acoustic classification. One approach is based on recognition of resonance signatures. The approach considered here is based on imaging. The question to be addressed is the quality of the image of a buried mine. It is reasonably assumed that the intervening sediment will have a detrimental effect on the image quality.

The extent to which the intervening sediment will degrade the acoustic image of a buried mine is unknown at present. A number of physical mechanisms should be considered. Dispersion and signal decorrelation are two mechanisms that may cause blurring, but due to an almost total lack of experimental information, neither will be considered in this report. Three mechanisms are considered here.

(1) Ghosting: In transmission from water into sediment, more than one type of wave may be generated. Each wave type travels at a different speed and is capable of producing an image. The superposition of images from more than one wave type may cause ghosting.

(2) Warping: The water-sediment interface is often rippled and the sediment itself is often inhomogeneous, causing distortion of the acoustic raypaths. The effect is to warp the image.

(3) Fogging: Granular sediments, such as sand, inherently have high volume scattering strength. Muddy sediments may acquire a high volume scattering strength due to inclusions, such as gas bubbles. The resulting diffuse scattering generates a background reverberation, analogous to fog in visual images. The result is a degradation of image quality as a function of burial depth and grazing

angle. The objective is to develop a capability to quantify these environmental effects on acoustic imaging.

2. GHOSTING

Ghosting may happen as a result of multipath propagation or when two or more types of waves, traveling at different speeds, interact with the target. Multipath effects are well understood and may be avoided in most cases. The problem of multiple wave types is less well known. The ocean sediment consists of solid material saturated with sea water. In accordance with Biot's theory, an acoustic wave impinging on the water-sediment interface generates up to three waves in the sediment, two compressional waves and a shear wave. The compressional waves are usually referred to as the "fast" and "slow" waves. The three waves travel at different speeds.

In soft muddy sediments, one compressional wave is dominant and the medium may be approximated as a liquid; a sound wave passing through a water-mud interface is simply refracted.

Ghosting is more likely to occur in a sandy sediment because it can support all three wave types. Referring to a model of sandy sediments by Chotiros,[2] the relative amplitudes of sediment penetrating fast, slow, and shear waves are computed as a function of depth, at selected grazing angles, and at a frequency of 20 kHz. Figure 1 illustrates the problem. The model input parameters are taken from the first column of Table III in reference 2, representing a sandy sediment found off Panama City, Florida. Referring to Fig. 1(a), the dominant sediment penetrating wave, at a grazing angle of 40°, is the fast wave. The shear wave is at least 60 dB lower than the compressional waves and may be safely ignored. At depths less than about 0.15 m, there is a possibility of ghosting because the slow wave is only a few decibels less than the fast wave. An image produced by the fast wave may be accompanied by a weaker slow wave image. The fast wave image would arrive earlier than that of the

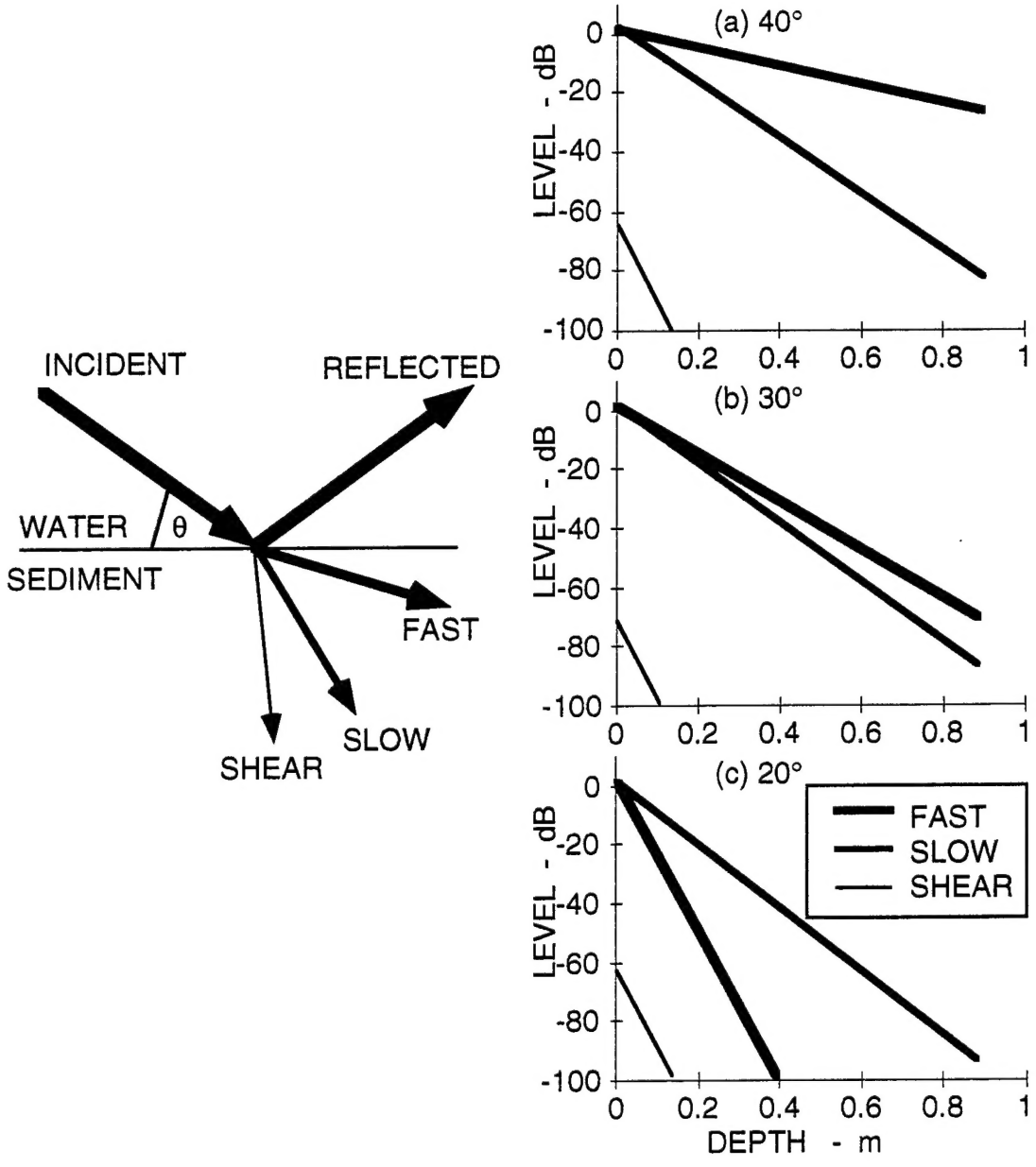

Figure 1

Acoustic pressure and shear stress levels as a function of depth, at 20 kHz in sand, in response to a 0 dB incident acoustic plane wave at grazing angles (a) 40°, (b) 30°, and (c) 20°.

slow wave, producing a trailing ghost image. Referring to Fig. 1(b), at a grazing angle of 30°, the fast and slow wave amplitudes are almost equal and ghosting is likely at all depths. At 20°, as shown in Fig. 1(c), the slow wave is expected to be stronger than the fast wave, giving a leading ghost image.

There is a further complication because the refraction angles of the fast and slow waves are very different. The two types of waves would strike the target at different angles of attack and are unlikely to be scattered from the same target features. The fast and slow wave images would appear rotated but by different angles, due to the differences in refraction angles. An illustration is shown in Fig. 2 of a rather irregularly shaped target, rather like a wing with a hump running along its center line. In this illustration, the corner C is only visible in the slow wave image; the fast wave raypath to C is blocked by the hump.

3. WARPING

The water-sediment interface is often rippled due to the action of water currents near the bottom. The apparent refraction angle of sediment penetrating sound rays would be dependent on the local slope at each point on the water-sediment interface in the down- and cross-range planes, respectively. This is illustrated in Figs. 3 and 4. The resulting image would appear warped. The severity of the problem depends on the magnitude of the large scale roughness of the interface. The roughness wave-number spectrum of water-sediment interfaces has been measured at a number of sites by Briggs.[3] Two sites were chosen, a sandy site referred to as Mission Bay II and a muddy site, Arafura Sea. Measurements from these sites are used to estimate image warping as an illustration. Let us consider the same target as in the previous illustration, imaged at a grazing angle of 20°.

To be realistic, it is also necessary to postulate a sonar that, under ideal conditions, would give images of acceptable resolution at a useful range; for example,

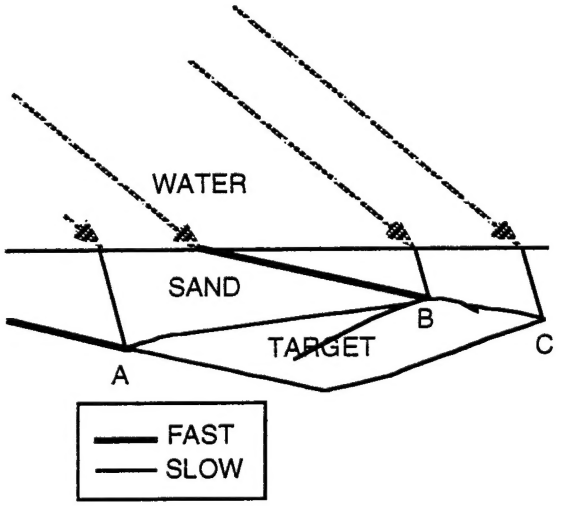

Figure 2
Illustration of ray paths of fast and slow waves to scattering points of a buried target.

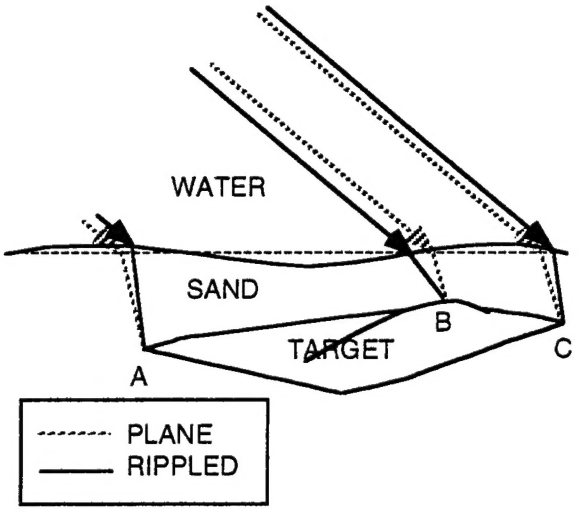

Figure 3
Illustration of warping in the down-range direction by deflection of raypaths due to ripples in the water-sediment interface.

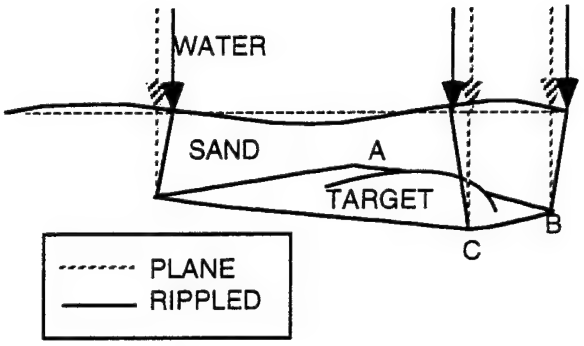

Figure 4
Illustration of warping in the cross-range direction by deflection of raypaths due to ripples in the water-sediment interface.

10 cm and 500 m, respectively, for resolution and range. For the sake of argument, let us consider a sonar operating at a frequency of 100 kHz, with a bandwidth of 50 kHz, and a horizontal aperture of 20 m. The large aperture is necessary to achieve the desired resolution at the stated range. How such a large aperture is achieved is outside the scope of this paper. Finally, it is assumed that the sound rays reaching the buried target enter the sediment at a grazing angle of 20°.

Using measured wave-number roughness spectrum as input, the surface tilt statistics were computed using methods developed previously for numerical computations of reflection loss from a rough water sediment interface.[4] The roughness may be divided into two components, a small scale component which causes a blurring of the image that further degrades the resolution of the sonar, and a large scale component which causes the warping. The predicted warp statistics, in terms of the root-mean-square deviation of the image from its undisturbed condition, are shown in Figs. 5 and 6 as a function of grazing angle for targets 3 m and 30 cm deep in the mud and sand sediments, respectively. These burial depths were chosen to give a two-way signal attenuation of about 50 dB at a grazing angle of 20°, which is likely to be the limit for buried target detection and imaging. In the muddy sediment, with a wave speed of 1400 m/s, it is evident that the cross-range warp is the larger one and is predicted to peak near 30°. In Fig. 6, the results for both the fast and slow waves in sand are shown. The fast and slow wave images are predicted to be dominant above and below the critical grazing angle, respectively; the critical grazing angle is in the region of 30°. For the fast wave (1700 m/s), the down-range warp is predicted to increase rapidly as the critical angle is approached. The slow wave (1100 m/s), which is dominant below the critical angle, is predicted to produce a relatively undistorted image.

To illustrate the significance of warping, the statistics were used to realize a warped image of a target buried 3 m deep in the muddy sediment, as shown in Fig. 7. The warped image is shown superimposed on the perfect image. In addition, the

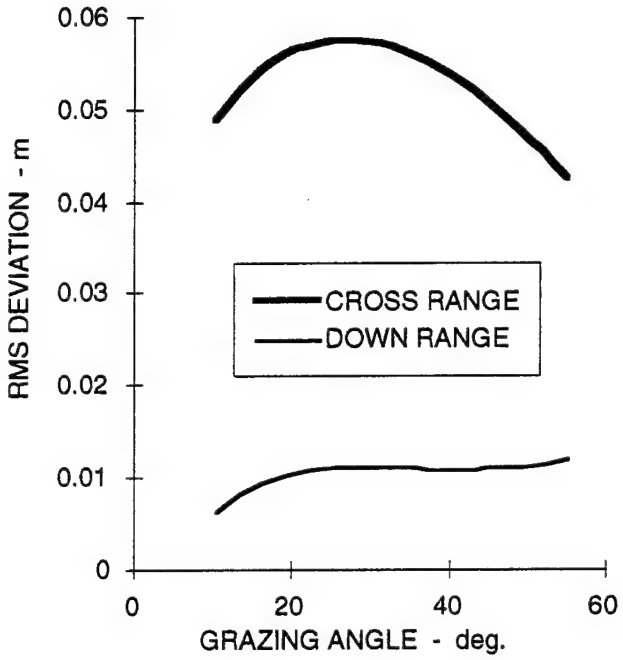

Figure 5
Estimated image warping statistics of 3 m deep target in a muddy sediment as a function of grazing angle.

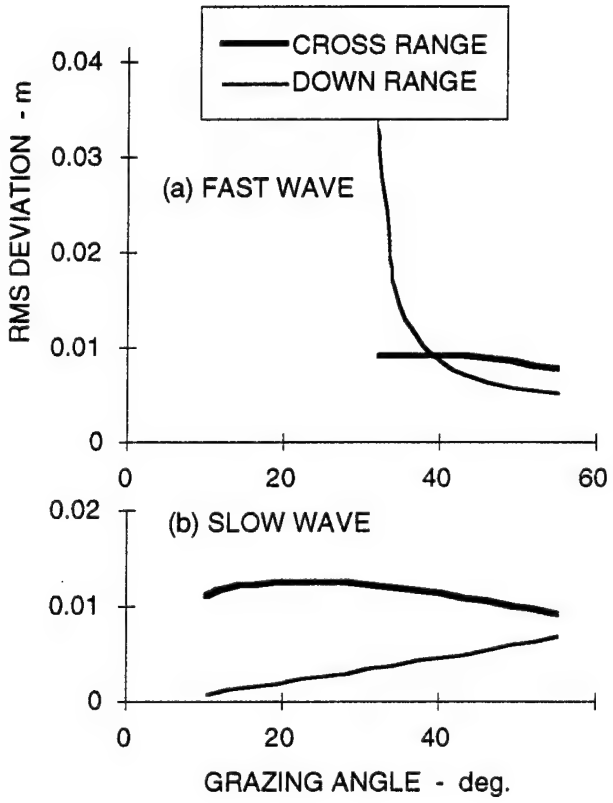

Figure 6
Estimated image warping statistics of 30 cm deep target in a sandy sediment as a function of grazing angle, for (a) fast and (b) slow wave images.

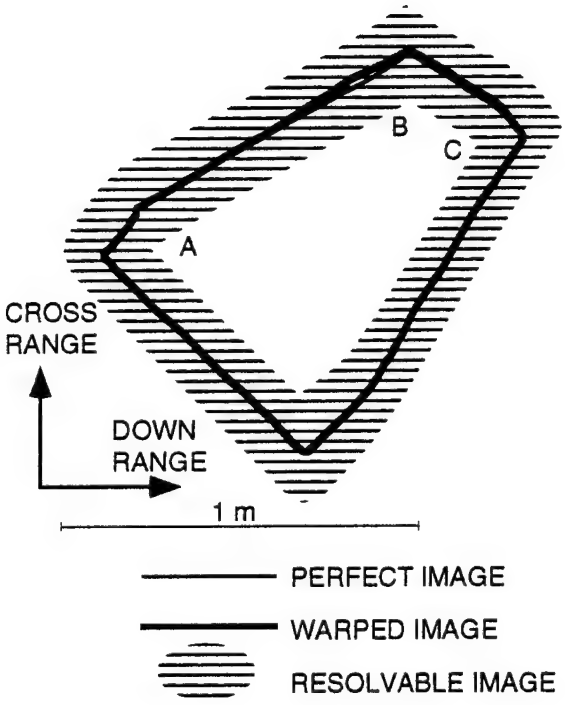

Figure 7
Illustration of image warping of a target 3 m deep in a muddy sediment.

resolvable image, due to sonar resolution and the blurring effect of small scale roughness, is shown in the background. It is evident that the warp is small compared to the resolution limits. Only the effects due to surface roughness have been considered. Volume inhomogeneities have not been considered because of a lack of sufficient data.

4. FOGGING

Image fogging is caused by diffuse volume scattering from the sediment. The mechanism is not well understood. There is some uncertainty regarding the correct scattering theory, i.e., single or multiple scattering. It is likely that in soft muddy sediments, a single scattering approximation is appropriate because scattering is not intrinsic to the mud but mainly caused by discrete inclusions. In sandy sediments, multiple scattering may be appropriate because the scattering is intrinsic to the sand grains. The effect is akin to that of fog in optical imagery.

An estimate of the fogging problem for a sandy sediment is demonstrated as follows. The net effect of sediment backscattering is expressible in terms of the bottom backscattering strength. A typical value for backscattering strength at 20° may be estimated from the extant database[5] of measured values at 10°, (BS_{10} = -33 dB), giving BS_{20} = -27 dB at 20° assuming Lambert's rule. The expected signal-to-backscatter ratio is given by

$$SNR = TS_A - 2TL - 10\log(A) - BS_{20} \quad ,$$

where TS_A is the target strength of prominent elements of the target within a sonar resolution cell of area A and TL is the transmission loss. For this illustration, a reasonable assumption is a TS_A of -20 dB along the edge of the target; from Fig. 1(c) 2TL increases with depth at a rate of 170 dB/m. A is the resolution area of the sonar, assumed to be 10 cm by 10 cm. Using these values, it is computed that at a depth of

3 cm, the SNR will be 23 dB; at 15 cm, the SNR drops to only 3 dB. Assuming a log-normal standard deviation of 5.7 dB in the backscattering,[6] a simulation of the fogging effect at these values of SNR is shown in Fig. 8. The ability to image is lost somewhere between 3–15 cm.

5. EXPERIMENT

An experiment was devised to study the effect of burial on acoustic imaging quality. A focused receiving array, operating between 100–200 kHz, was constructed and mounted on a rail over the Applied Research Laboratories, The University of Texas at Austin (ARL:UT) sand tank. It is a curved PVdF array, with a 5.5 m radius of curvature, and an aperture of 2.4 m. It was used with an existing square (0.254 m x 0.254 m), wideband projector, made of a 1-3 composite material (15% PZT-4 in a Shore D80 PU matrix, poled and connected by silver epoxy electrodes, made by Material Systems, Inc.) capable of operating between 20–200 kHz with little distortion. The system has a nominal resolution of 2 cm down- and cross-range. A photograph of the arrays is shown in Fig. 9.

To observe the degradation in imaging resolution as a function of burial depth, the sonar was tested on a number of small targets buried at various depths. This was accomplished by attaching a row of ping-pong balls to a stainless steel bar and inserting the assembly, using a water jet, into the sediment at an angle of approximately 45°. A photograph of the exposed part of the assembly is shown in Fig. 10. In addition, a fluid-filled sphere was also placed on the sand surface for reference. The sonar was deployed from a column on a motorized platform at a height of approximately 2 m above the sand bed, as shown in Fig. 11(a). The projector beam was directed towards the targets. The receiver array was angled so that the targets were always in its focal zone as the beam was scanned over the target area by the motorized platform, as shown in Fig. 11(b). A detailed diagram of the target arrangement is shown in Fig. 12. The projected vertical beam pattern of the array, at

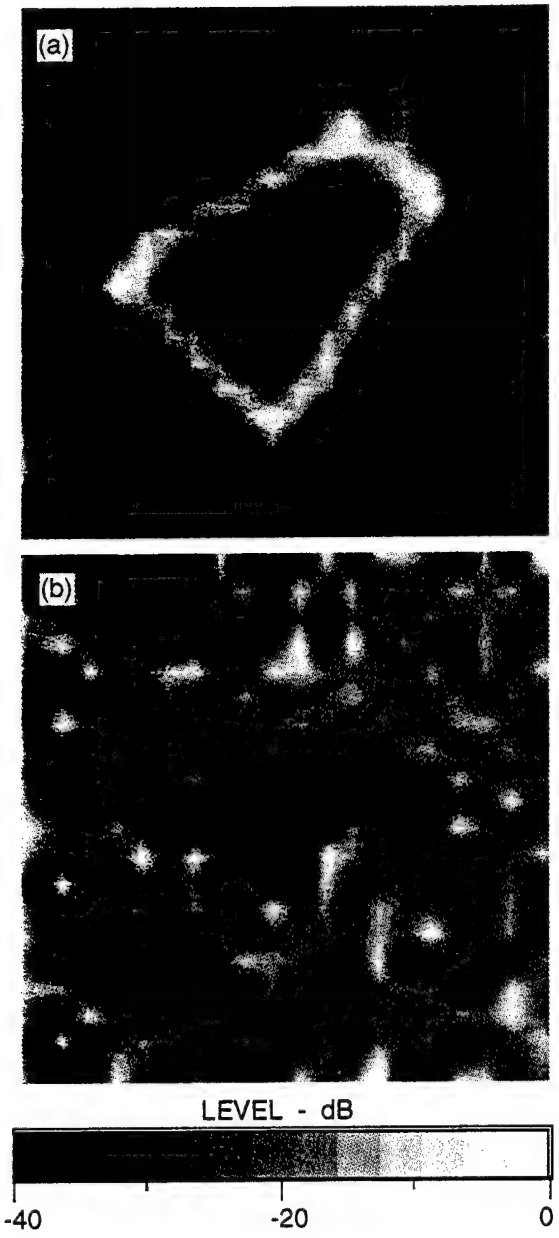

Figure 8
Image degradation due to fogging in a sandy sediment at depths (a) 3 cm and (b) 15 cm.

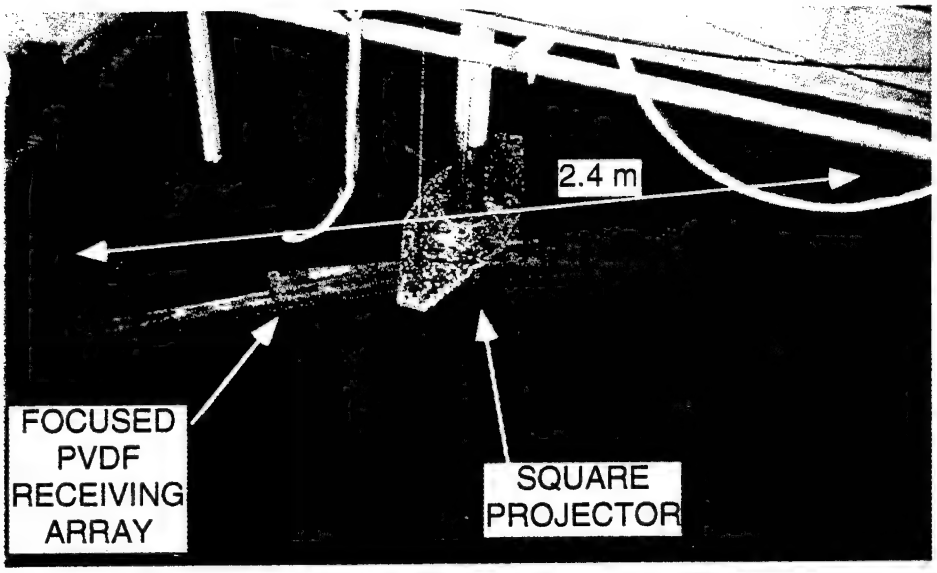

Figure 9
Photograph of experimental acoustic arrays.

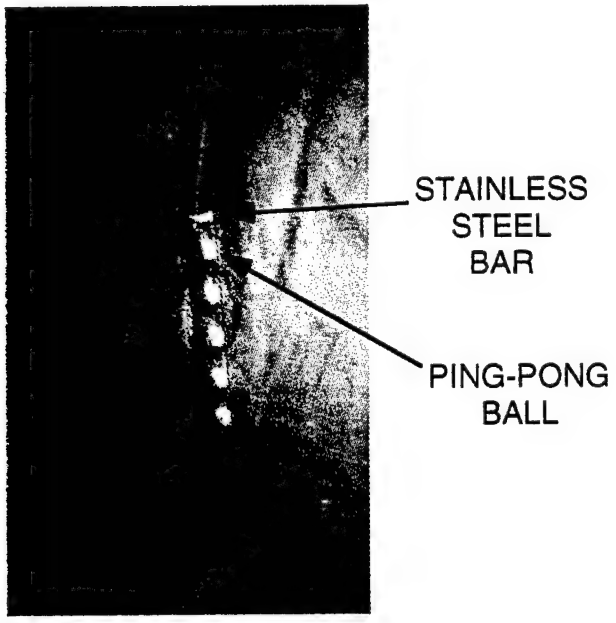

Figure 10
Photograph of target array.

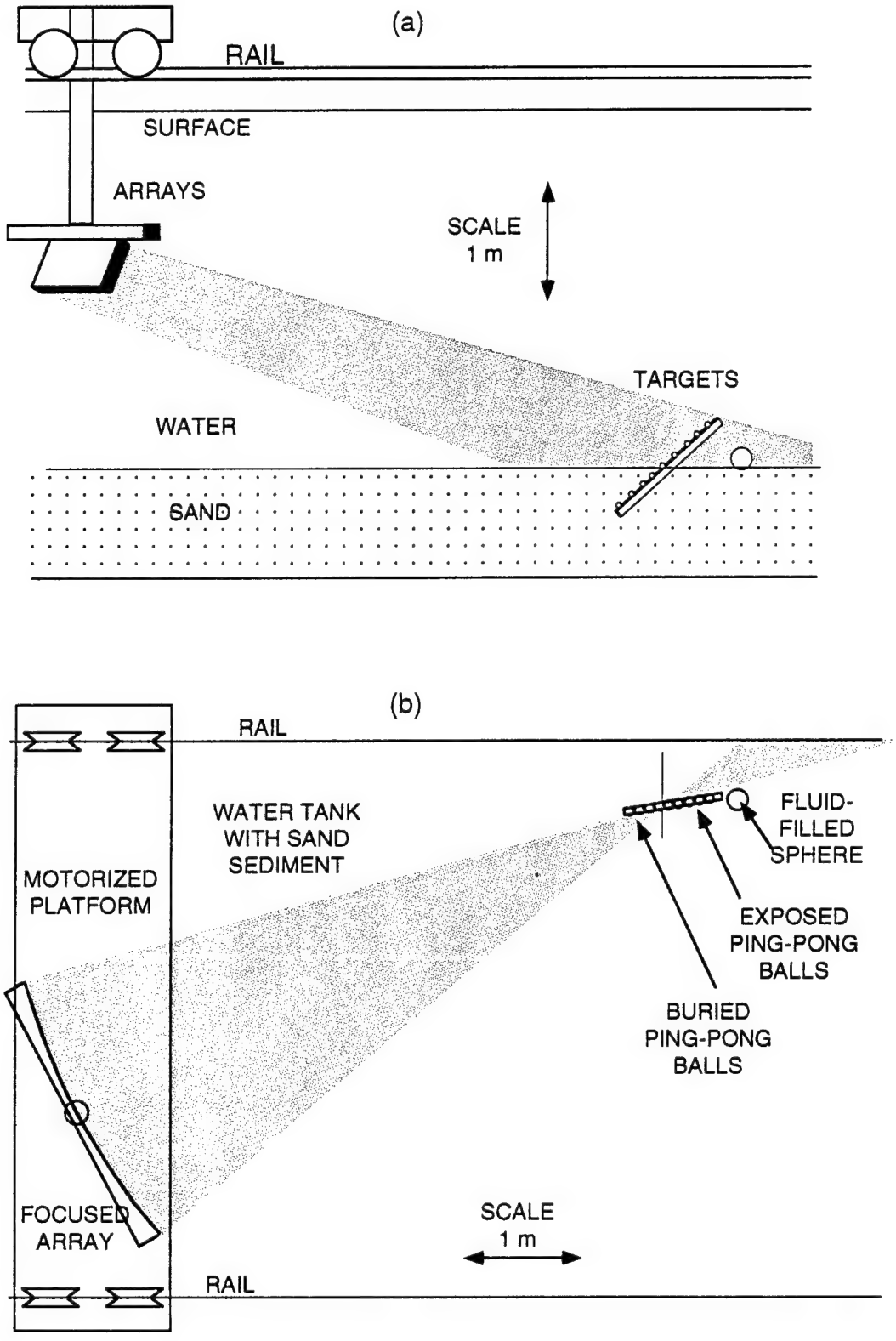

Figure 11
Experiment: (a) vertical section and (b) plan view.

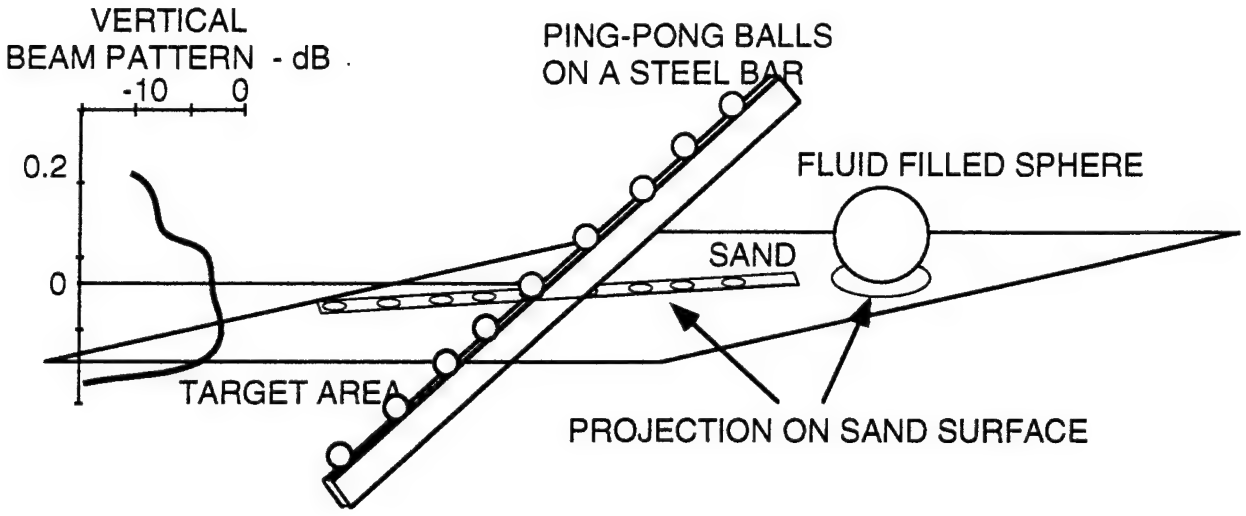

Figure 12
Configuration of targets and projected vertical sonar beam pattern.

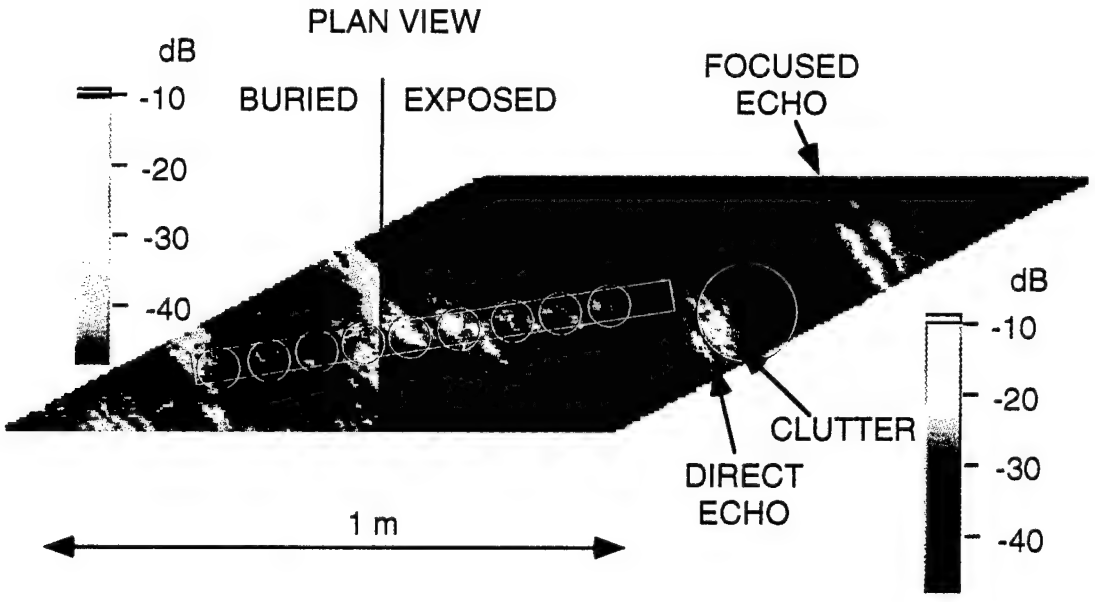

Figure 13
Acoustic imaging results.

the target position, was also measured to verify that there was adequate vertical coverage for detection of both exposed and buried targets. By sweeping the sonar beam horizontally over the target area, an acoustic image was constructed, as shown in Fig. 13.

The image obtained shows the exposed targets quite clearly. The echo from the front of the fluid-filled sphere is immediately followed by clutter due to bottom interaction. At a distance of approximately one diameter behind the sphere, the focused echo is detected. It too is accompanied by bottom clutter. A weak echo is observed from the top corner of the stainless steel bar that supports the ping-pong balls. There are numerous echoes from the exposed ping-pong balls. In the left half of the image, the buried ping-pong balls are just detectable, but the reduced signal levels required a more sensitive intensity scale. The shallowest buried ping-pong ball has the strongest echo but the echo appears to be fragmented. Unfortunately, it is not possible to draw any conclusions regarding image degradation from this data set, because the exposed ping-pong ball echoes appear to be as deranged and fragmented as those of the buried ones. It can be said that, for the conditions of this experiment, burial caused a significant reduction target echo level, but the distortions caused by burial were not a significant factor in image degradation. The most noticeable sediment acoustic effect is the clutter that accompanies the echoes from targets that are very close to, or resting on, the sand surface. This is thought to be due to multiple reflection and scattering between target and the water-sediment interface.

6. CONCLUSIONS

Of the physical mechanisms that can potentially degrade buried target imaging, three were investigated: ghosting, warping, and fogging. From the example calculations in this paper, it is evident that warping is expected to be insignificant. Ghosting is not applicable to soft muddy sediments, but may be a problem in sandy sediments, depending on grazing angle. Fogging, due to backscattering from the

sediment, is expected to be the limiting factor. The laboratory experiment demonstrated the reduction in signal level due to burial, but the above mentioned mechanisms of image degradation were overshadowed by other processes, particularly the apparent fragmentation of the echoes from both buried and exposed targets and clutter caused by multiple reflections between target and water-sediment interface. Follow-on work should address the environmental effects that are responsible for the echo fragmentation and clutter in addition to the degradation due to burial.

ACKNOWLEDGMENTS

Thanks are due to Steve Stanic and Dan Ramsdale for encouragement and support. This work was sponsored by Naval Research Laboratory, Stennis Space Center, under the Environmental Physics for MCM Program.

REFERENCES

1. M. A. Biot, "General solutions of the equations of elasticity and consolidation for a porous material," J. Appl. Mech. 91-96 (March 1956).

2. N. P. Chotiros, "Biot model of sound propagation in water-saturated sand," J. Acoust. Soc. Am. 97(1), 199-214 (January 1995).

3. K. B. Briggs, "Microtopographical Roughness of Shallow-Water Continental Shelves," IEEE J. Oceanic Eng., 14(4), 360-367 (October 1989).

4. N. P. Chotiros, "Reflection and Reverberation in Normal Incidence Echo-Sounding," J. Acoust. Soc. Am. 96(5), 2921-9 (November 1994).

5. N. P. Chotiros and F. A. Boyle, "A new high-frequency ocean bottom backscattering model," J. Acoust. Soc. Am. Vol. 96, No. 5, Pt. 2, 3264 (November 1994).

6. H. Boehme, et al., "Acoustic backscattering from the ocean bottom," Applied Research Laboratories Technical Report No. 84-8 (ARL-TR-84-8), Applied Research Laboratories, The University of Texas at Austin (March 1984).

9 September 1997

DISTRIBUTION LIST
GR-AS-97-03
Group Report under Contract N00039-91-C-0082
TD No. 01A3095, High Frequency Buried Target Imaging

Copy No.	
	Commanding Officer Naval Research Laboratory Stennis Space Center, MS 39529-5004
1-3	Attn: D. Ramsdale (Code 7170)
4	S. Stanic (Code 7174)
5	D. Lott (Code 7431)
6	S. Tooma (Code 7430)
7	R. Meredith (Code 7174)
8	Library (Code 7032.2)
	The Office of Naval Research San Diego Regional Office 4520 Executive Drive, Suite 300 San Diego, CA 92121-3019
9	Attn: J. Starcher (ACO)
	Director Naval Research Laboratory Washington, DC 20375
10	Attn: E. Franchi (Code 7100)
11	B. Houston (Code 7136)
	DTIC-OCC Defense Technical Information Center 8725 John J. Kingman Road, Suite 0944 Fort Belvoir, VA 22060-6218
12 - 23	Attn: Library

Distribution List for GR-AS-97-03 under Contract N00039-91-C-0082, TD No. 01A3095 (cont'd)

Director
Research Program Department
Office of Naval Research
Ballston Tower One
800 North Quincy Street
Arlington, VA 22217-5000

24 Attn: J. Simmen (Code 321)
25 E. Chaika (Code 322)

Commander
Dahlgren Division
Naval Surface Warfare Center
Dahlgren, VA 22448-5000

26 Attn: Library

Director
Applied Physics Laboratory
The University of Washington
1013 NE 40th Street
Seattle, WA 98105

27 Attn: D. Jackson
28 K. Williams
29 S. Kargl

Director
Life Sciences Directorate
Office of Naval Research
Arlington, VA 22217-5000

30 Attn: S. Zornetzer (Code 114)

Director
Marine Physical Laboratory
The University of California, San Diego
San Diego, CA 92152

31 Attn: C. de Moustier

Commander
Mine Warfare Command
325 Fifth St. SE
Corpus Christi, TX 78419-5032

32 Attn: G. Pollitt (N02R)

Distribution List for GR-AS-97-03 under Contract N00039-91-C-0082, TD No. 01A3095 (cont'd)

	Applied Research Laboratory The Pennsylvania State University P.O. Box 30 State College, PA 16804-0030
33	Attn: D. McCammon
	National Center for Physical Acoustics University of Mississippi Coliseum Drive University, MS 38677
34	Attn: J. Sabatier
	Commanding Officer Coastal Systems Station, Dahlgren Division Naval Surface Warfare Center Panama City, FL 32407-5000
35	Attn: R. Lim (Code 130B)
	Commander Naval Undersea Warfare Center Division New London, CT 06320-5594
36	Attn: P. Koenig (Code 33A)
37	Frank Boyle, ARL:UT
38	Nicholas P. Chotiros, ARL:UT
39	John M. Huckabay, ARL:UT
40	Library, ARL:UT
41-46	Reserve, ARL:UT